Wetting and Capillary Phenomena of Water on Mica

Lei Xu,† Anna Lio, Jun Hu,† D. Frank Ogletree, and Miquel Salmeron*

Materials Sciences Division, Lawrence Berkeley National Laboratory, University of California, Berkeley, California 94720

Received: July 14, 1997; In Final Form: November 14, 1997

The structure of water films on mica was locally modified by contact with the tip of an atomic force microscope (AFM) in a humid environment. The subsequent evolution of the film was studied by noncontact scanning polarization force microscopy. At high relative humidity (>20%), capillary condensation caused water to form droplets and two-dimensional islands around the contact point. The droplets evaporated in a short period of time, but the islands remained for much longer periods (hours). At low relative humidity (<20%), the tip contact produced a circular depression in the local polarizability. None of these structures could be observed in contact AFM images which revealed only the usual atomically flat mica surface.

Introduction

The formation of water films on surfaces of materials exposed to humid environments is a well-documented fact of nature and the basis of many capillary phenomena. It plays a crucial role in biological phenomena, wetting, corrosion, etc. These water films, often of molecular dimensions, have been studied by means of adsorption isotherms,[1,2] ellipsometry,[3] NMR,[4] surface forces apparatus (SFA),[5,6] and other techniques.[7,8] Molecular scale information about water monolayers formed at low temperature on metal surfaces has been obtained with ultrahigh-vacuum surface science techniques, including low-energy electron diffraction, high-resolution energy loss spectroscopy,[9] and scanning tunneling microscopy (STM).[10] A review of water adsorption on surfaces can be found in the work of Thiel and Madey.[11]

The spatial distribution of water, and liquids in general, is determined by their wetting properties and has received considerable attention, particularly from the theoretical point of view.[12,13] Most experimental studies have been conducted using optical techniques whose spatial resolution is diffraction limited to the micrometer range.[14,15] At the nanometer scale, however, such studies have not been possible until now, due to the limitation of current microscopy techniques. Thanks to the development of scanning polarization force microscopy (SPFM),[16] we can image the structure and properties of films formed by water on surfaces exposed to humid air at room temperature.[17,18] SPFM has also been used to image other liquids with nanometer resolution, including acids, bases, and salt solutions.[19−21]

In this paper we present new results from our studies of the structure of molecularly thin water films. In particular, we will show that the AFM tip can be used as a probe to perturb the water film locally (on the micrometer to nanometer scale) following a gentle mechanical contact with the surface. At high humidity, this contact facilitates the deposition of water by virtue of the capillary condensation around the contact point.

Experimental Section

The experiments were performed in a homemade AFM, enclosed in a humidity-controlled plastic box. The room temperature was 20−23 °C, as measured with a Hg thermometer. The relative humidity (RH) in the box was increased by evaporating water from a beaker or decreased by insertion of a desiccant material and by flow of dry N_2 gas. It was measured by an RH-20C Omega hygrometer. We used a commercial scanning probe control electronics from RHK Technology, Inc. The cantilevers, from Digital Instruments, had a nominal force constant of 0.58 N/m. They were made conductive by coating them with Pt, 100−500 Å thick. The tips were pyramidal in shape, and the radius of the apex varied between 100 and 1000 Å.

When the AFM is operated in the SPFM mode, the tip is biased to a few volts using dc or ac power supplies. Attractive electrical forces due to polarization of the sample are measured when the tip is located at a distance of a few hundred angstroms. This force is stabilized by the feedback control. Typical values of the force are 1−10 nN for a bias of ±1 to ±5 V. The tip height during imaging is between 100 and 300 Å. Additional details of the operation of the SPFM can be found in our previous papers.[16,17,19]

We used muscovite mica in all our experiments. The samples were cut in the form of disks ∼1 cm in diameter and cleaved to a thickness of a few tenths of a millimeter. They were either glued to a metallic substrate using conductive epoxy or simply attached with double-sided adhesive tape.

In the experiments, the tip was brought into contact with the mica surface for a controlled amount of time and at a given applied force. To that effect, the feedback control of the AFM electronics was disabled, and a linear *z* excursion was applied to the sample toward the tip while monitoring the lever deflection. The excursion was stopped just after the jump to contact point, with a value of the external load around zero, within a few nanonewtons. The contact time was varied from milliseconds to minutes. After the desired contact time had elapsed, the tip was retracted and noncontact SPFM images were acquired to monitor changes in the surface. Because of the low applied load, the contact area should have a radius of only a

† Permanent address: Shanghai Institute of Nuclear Research, Chinese Academy of Sciences, P.O. Box 800-204, Shanghai 201800, P. R. China.
* Corresponding author. E-mail: salmeron@stm.lbl.gov.

S1089-5647(97)02289-X CCC: $15.00
Published on Web 01/15/1998

few nanometers, as estimated from the elastic Hertzian model.[22] During contact, the tip bias voltage was always turned to zero.

In dry environments (RH < 20%), the surface potential of mica immediately after cleavage is very high (>10 V) and might last for several hours, making SPFM imaging almost impossible during that time. This very high surface potential is in part due to a charge unbalance, such as would arise, for example, from a loss or an uneven distribution of K^+ ions between the two cleavage faces. In experiments performed with mica cleaved in ultrahigh vacuum (10^{-10} Torr), discharging was found to require more than 24 h.[23] At a RH > 20−30%, however, the surface potential due to this electrostatic charging is reduced to almost neutral in a few seconds (within 0.5 V) due to the increased mobility of hydrated surface ions. All the experiments reported here were conducted after allowing this initially high surface potential to disappear by cleaving the mica at 30−40% RH and then readjusting the humidity to the desired level.

An important point about the tips that was overlooked in our previous experiments is the frequent loss of the metallic coating in a small area around the apex due to wear or damage. This was determined by measuring the electrical tip−surface contact resistance on gold substrates. These tip defects did not affect significantly the performance of the microscope, in either attractive or contact modes, but were important in the capillary phenomena induced by the tip−surface contact discussed here. The amount of water deposited, and the extent of the area it covers on the surface, depends on the wetting properties of the tip, in addition to those of the sample. It appears that the exposed silicon nitride or oxide termination at the tip apex is hydrophilic and thus capable of affecting the substrate much more dramatically than a pure Pt termination, which is far less hydrophilic.

Results

As we reported recently, in ambient conditions, water condenses on mica forming flat, two-dimensional films.[16,17] The stability of these films is the result of the strong binding of water on mica due to its polar nature. Usually no contrast can be seen in SPFM images, which implies that the water molecules are adsorbed uniformly (on the scale of nanometers) on the surface. According to ellipsometry results,[2] the average thickness of the water film is ∼2 Å, when the RH is ∼50%.

Capillary Forces between Tip and Surface during Contact. The presence of water manifests itself dramatically in the force that is necessary to separate the tip from the surface after establishing contact. This force is referred to as the pull-off force F_{off} in the AFM literature. It has several contributions, including short-range tip−surface adhesive forces, van der Waals forces, and forces resulting from capillary condensation of water around the contact point. This last contribution arises from the formation of a concave meniscus around the contact, giving rise to a negative Laplace pressure.[24] It often constitutes the strongest part of the pull-off force in humid environments. Experimental measurements of the pull-off force as a function of humidity for a tip of ∼200 Å radius are shown in Figure 1. As we can see, the force is small (∼2 nN) and constant when the humidity is <20%. It increases rapidly at 20% RH and reaches its highest value between 20 and 40%. A continuous decrease is observed afterward, up to the highest values of 90−95% RH. Similar results were obtained with tips of different radii, although the value of the forces scaled up with tip radius.

Another related observation is the finite buildup time of the capillary force during contact. At high humidity (>20%), the pull-off force increases with time, as shown in Figure 2. For the particular tip radius used in the experiment, the force is 87 nN after 1 ms contact at 42% RH. It slowly increases until it saturates at ∼100 nN after 10 s contact. Interestingly, when the humidity is <20%, a decrease in the pull-off force is observed, as shown in the same figure for a relative humidity between 8 and 12%.

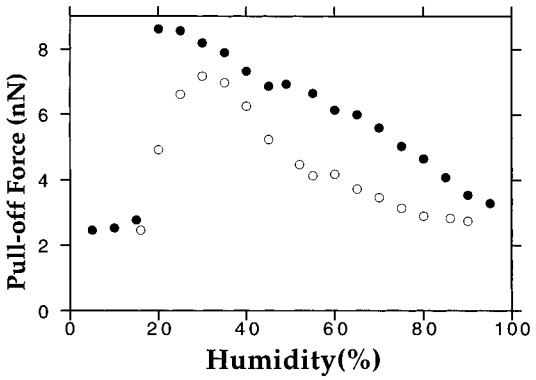

Figure 1. Pull-off force F_{off} between a hydrophilic Si_3N_4 tip and the mica surface as a function of the relative humidity (RH) at room temperature. The spring constant of the lever is 0.1 N/m. Estimated tip radius is ∼200 Å. Some variability in the value of F_{off} is observed, as seen in the two sets of data points acquired during increasing (open circles) and decreasing (closed circles) humidity.

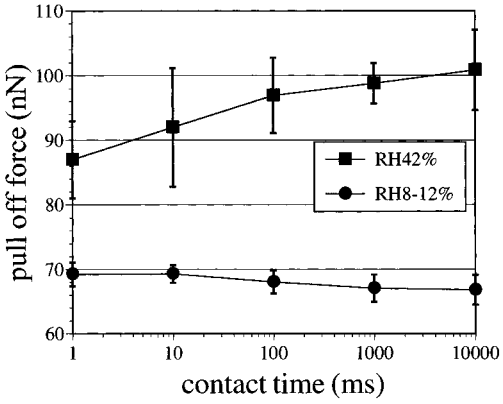

Figure 2. Dependence of the pull-off force on the duration of the contact time. When the humidity is >20%, an increase with time is observed. At 42% RH, it saturates after ∼10 s. Below 20%, a decrease is observed which also saturates after a several tens of seconds.

Formation of Residual Films and Droplets. After breaking the contact, we immediately proceeded to image the surface in the SPFM mode. We found that the structure of the surface in the area surrounding the contact point had been significantly altered. At sufficiently high humidity, some of the water accumulated in the capillary meniscus was left behind on the mica in the form of a droplet. Usually this droplet will spread rapidly and/or evaporate. However, on samples that had been rendered slightly hydrophobic by some contamination, the droplet remained on the surface long enough to be imaged, as shown in the example of Figure 3. In this case, the mica substrate was exposed to laboratory air for a couple of hours before the contact. At the humidity level of this experiment (58%), it took about 4 min for the droplet to evaporate. Profiles of the shrinking droplet are shown at the bottom of the figure. In addition to the droplet, flat structures are visible in its vicinity. These are residual layers of water left behind by the receding/evaporating drop. These structures were called "phase II water" in our previous papers. On cleaner, freshly cleaved samples, only the phase II structures were visible after the contact, any droplet left after tip retraction probably having spread or evaporated too fast to be observed.

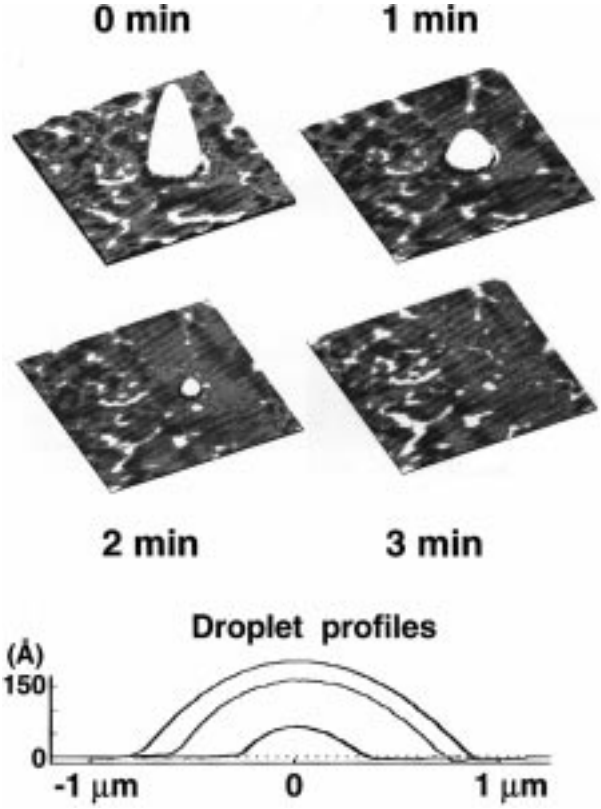

Figure 3. Noncontact SPFM images (6 μm × 6 μm) showing the evaporation of a droplet of water left on the surface of mica after breaking the capillary neck formed around the AFM tip during contact. The mica surface in this experiment was rendered slightly hydrophobic by exposure to air for a couple of hours. The droplets evaporate in a few minutes at 58% humidity. Their contact angle is ~2.6°. On freshly cleaved mica the droplets spread and/or evaporate too quickly to be imaged. Profiles across the droplets are shown at the bottom. Two-dimensional water structures can also be seen in the area surrounding the droplet.

Before presenting the results of imaging the water structures, we will describe experimental data on the frequency dependence of the polarization forces, which are important in the understanding of the origin of contrast in the SPFM images. After that, we present the imaging results grouped according to humidity regimes: low humidity (RH > 20%), medium RH (between 20 and 45%), and high RH (>45%).

Frequency Dependence of the Polarization Forces. The dependence of the polarization force on the frequency of an applied ac bias was studied in several different ways. In all cases, the tip was placed at a height of ~1000 Å. As a result of the ac voltage, the lever oscillates at a frequency which is twice that of the driving voltage. (The force is attractive in both the positive and negative cycles). The amplitude of these oscillations was measured as a function of the applied bias frequency. A set of data is shown in Figure 4. The sharp peak at 27 kHz is due to the excitation of strong cantilever oscillations when the driving frequency reaches half the value of the mechanical resonance of the lever. As can be seen, at a given frequency, the amplitude of the oscillatory force drops when the humidity decreases. The frequency at which the amplitude has decreased to half its dc or low-frequency value (cutoff frequency) is low enough at low humidity that even the scanning speed during imaging (~1 s/line) must be taken into account. Although not shown here, we also performed experiments in the time domain by measuring the time response of the lever deflection or force to a sudden change in the bias voltage. The same conclusions are reached using this method.

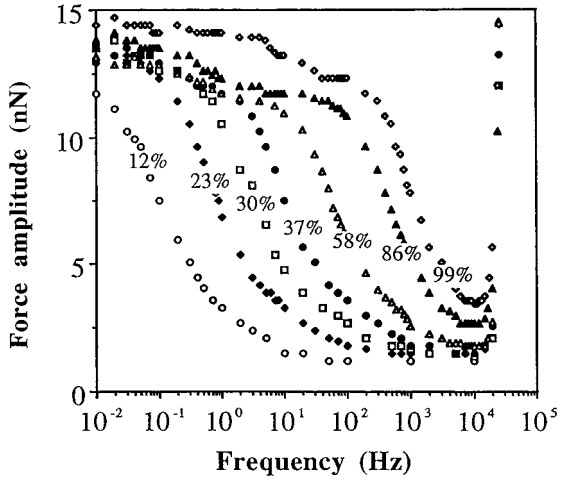

Figure 4. Frequency dependence of the amplitude of the ac electrostatic force between the AFM tip and the surface arising from the polarization of mobile surface charges. Each curve, represented by different symbols, corresponds to the value of the relative humidity indicated as a percentage. In this experiment, the tip was at a height of ~1000 Å. The applied ac-bias had an amplitude of 10 V p−p. Notice the shift of the curves to higher frequency as the humidity increases to near saturation. The sharp peak at 27 kHz is due to excitation of the mechanical resonance of the lever at 54 kHz.

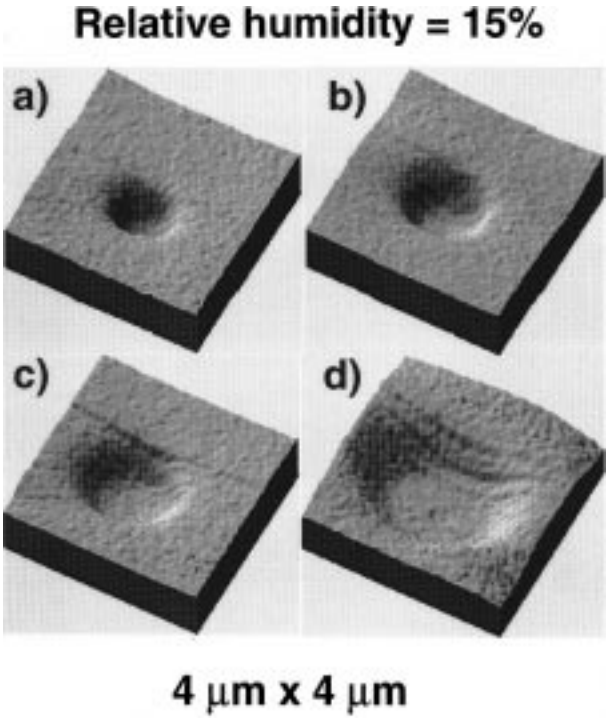

Figure 5. SPFM image (4 μm × 4 μm) acquired after the tip was in contact with the mica surface at 14% RH for (a) 2, (b) 5, (c) 10, and (d) 30 min. The "hole" in these images has an apparent depth of 130 Å. It is not a topographic hole but is due to the decrease of the electrostatic force in this area as a result of a lower surface polarizability, as discussed in the text. Contact AFM images of the same area reveal the usual atomically smooth mica surface with no apparent changes in its structure.

Imaging in the Low-Humidity (<20%) Regime. When the RH is <20%, physical contact of the tip with the surface produced a modified area with a circular shape, as observed in the subsequently acquired SPFM images. Figure 5 shows four SPFM images acquired after several contact experiments at ~15% RH for contact times of: (a) 2, (b) 5, (c) 10, and (d) 30 min. Each contact was performed on a new fresh area of the

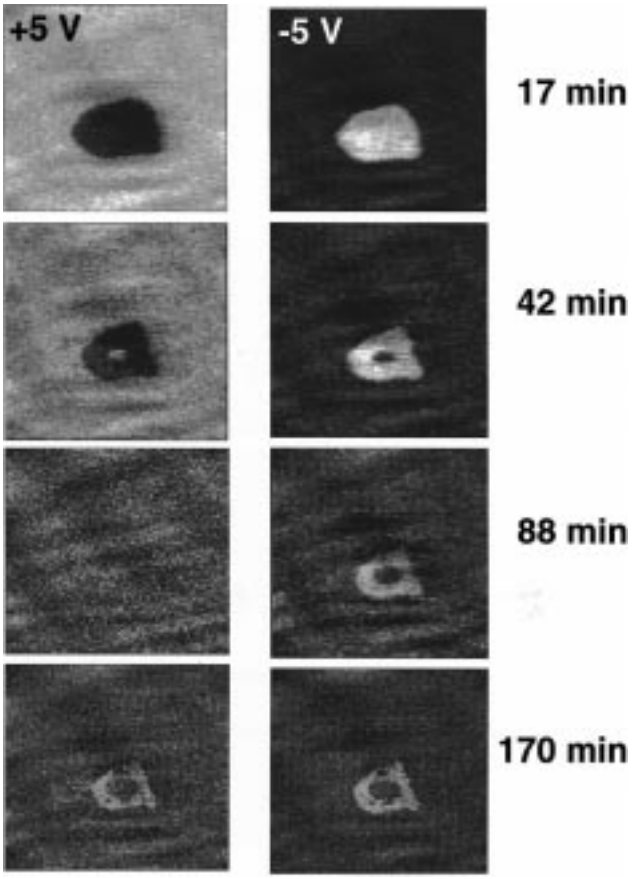

Figure 6. Time evolution of the SPFM images (7.8 μm × 7.1 μm) acquired with the tip biased with positive (left column) and negative voltages (+5 and −5 V). The humidity in the chamber is 35%. The top two images were acquired 17 min after a brief contact of the tip with the surface that produced the flat water island observed in the center. At positive bias, the island appears lower than its surroundings, while the opposite is true at negative bias. As time evolves, the island shrinks, its apparent height (or depth) decreases, and holes are formed inside. The contrast with the positive bias tip disappears and then reverses at ~80 min. After that, the contrast is always positive, i.e., a protrusion, for both bias signs.

mica surface. After a contact of two minutes, a circular "hole" of ~1 μm diameter was produced in the SPFM image, as shown in Figure 6a. The diameter of the "hole" increased monotonically with contact time, reaching 2.8 μm after 30 min of contact. The apparent depth of the hole is 50−130 Å, depending on the humidity, bias voltage, and height of the tip during SPFM imaging. Because of the sluggish frequency response at low humidity, it also depends on the scanning speed. However, the contrast or apparent depth does not depend on the sign of the bias. Contact AFM images acquired immediately afterward in the same area indicated that the mica remained atomically flat and indistinguishable from the original substrate. Therefore, the "hole" in the SPFM images indicates that a change in the local dielectric or polarizability properties of the mica has occurred. This change is also manifested in the frequency response of the polarization force when the tip is over the holes. At a scanning speed of 10 Hz, the apparent depth of the hole is ~100 Å; however, if we scan slower, e.g., 1.5 Hz, the hole is shallower. Also, at high frequency (we apply a 10 V amplitude, 1 MHz ac bias to the tip), the hole is much shallower or below the noise level of ~1 Å, as we have reported previously.[17]

The dielectric "holes" generated by the contact disappear with time: they become shallower and shrink in diameter until the surface again becomes dielectrically "flat" in the SPFM images,

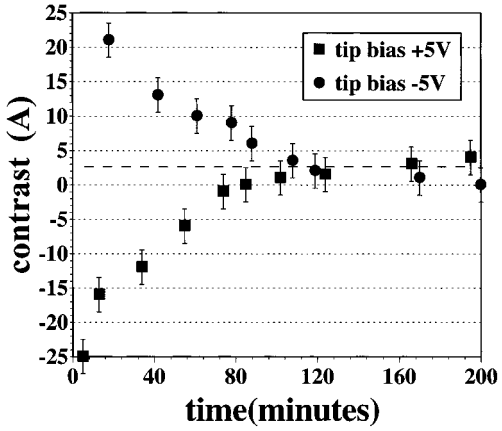

Figure 7. Plot of the apparent height and depth of the islands in the images of the previous figure as a function of time. Notice the contrast reversal of the positive images at ~84 min and the final steady-state contrast value of 2.5 Å observed for both tip polarities.

usually after several tens of minutes. At very low RH (<10%), holes disappear very slowly, while at 20% disappearance is too rapid to be observed.

Medium-Humidity (20−45% RH) Regime. *Contact Potential.* In contrast to the results obtained at low humidity, at humidity levels >20%, a very short contact (which can be much less than 1 s) produced a large modified area around the contact point. Again, this modification can only be imaged in the SPFM noncontact mode, while contact mode images show the usual, atomically flat mica surface. The size of the affected area increases with contact time from several hundred angstroms after a few milliseconds to tens of micrometers after several seconds. Flat, two-dimensional islands or patches appear in the affected region. As indicated above, we have referred to these as phase II water, while the surrounding, unperturbed water film was called phase I water.

The contrast between the two phases depends on the sign of the bias. The phase II islands appear lower, i.e., like a depression, with positively biased tips and higher (like an elevation) with negatively biased tips. This indicates that the electrical potential of the surface is higher inside phase II islands than outside them. Both the intensity of the contrast (apparent height or depth) and the size of the islands decrease with time, as shown in Figure 6. With negative bias, the island contrast is higher in absolute value than with positive bias by ~5 Å. After a sufficiently long time, however, the contrast becomes positive, i.e., a protrusion, for both polarities and equal to ~2.5 Å. A plot of the contrast evolution with time for the experiment in the previous example is shown in Figure 7. These results show that there are two contributions to the contrast: one which is polarity dependent and is due to contact potential differences and a second one which is independent of the sign of the bias and is responsible for the final 2.5 Å positive contrast. The first is the dominating contribution immediately after the contact, giving rise to apparent heights or depths in the tens of angstroms range. The second contribution, while small in freshly cleaved surfaces, becomes dominant after the contact potential difference between phase I and II has decreased sufficiently.

Island Size and Shape. In addition to the changes in surface potential, there are changes in the size and shape of the islands of phase II. Figure 8 shows a more detailed example of the evolution of the size and shape of the phase II patches produced after a contact of several seconds. Only the images taken at negative bias are shown here. In addition to edge mobility

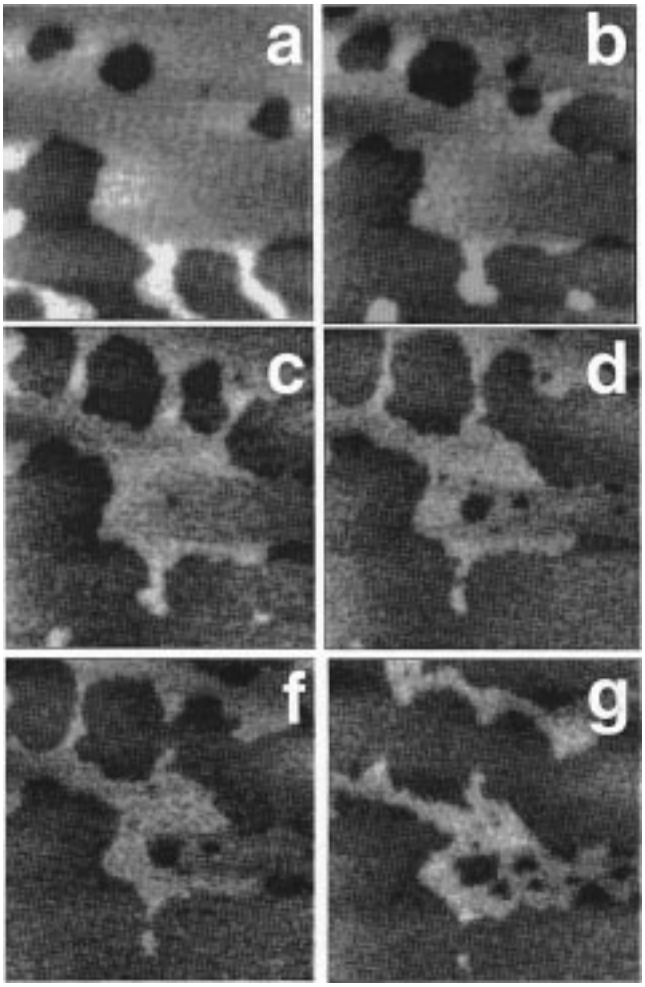

Figure 8. Evolution of the shape and size of the water structures formed after a tip contact of 5 s. The 3 μm $\times$ 3 μm SPFM images (a−g) were acquired with a negatively biased tip (−5 V) after (a) 30, (b) 50, (c) 70, (d) 130, and (e) 150 min. Notice the polygonal shape of many of the boundary lines separating phase II (bright) and phase I (dark).

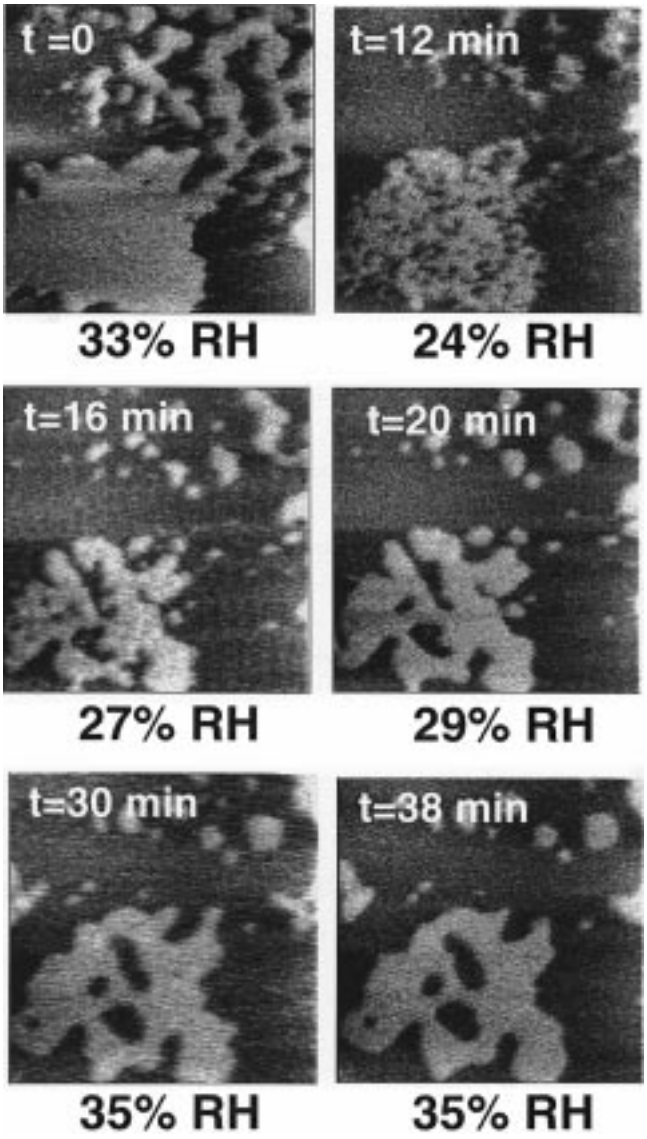

Figure 9. SPFM images (3.4 μm $\times$ 3.4 μm) showing the decrease in size of the water islands by shrinking and hole formation (two top images) and their subsequent recovery when the humidity is increased again (four bottom images). This is due to fast evaporation when the humidity is decreased from 33 to 24% and condensation when the humidity is increased to 27, 29, and 35%. The smaller holes formed due to evaporation refill completely while the island edges are also seen to advance. After 38 min, however, at 35% humidity, the recovery of the islands stops and then starts to slowly decrease in size again.

(advance and recession of boundaries), the area covered by phase II decreases by formation of holes in its interior. These holes become larger and more numerous with time until they finally percolate and cover the entire island area. It can also be seen that the shape of the boundaries between the two phases is often polygonal. By combining SPFM imaging with contact imaging to resolve the mica lattice, we have shown in previous work that the directions of the boundaries between the two water phases are closely related to the lattice orientation of the mica surface. Some of these polygonal edges can be seen clearly in the figure.

The disappearance of phase II is fast at low humidity and slow at high humidity. Partial recovery, i.e., an increase in size, also occurs if the humidity is increased as shown in Figure 9. By decreasing the humidity from 33 to 24%, numerous holes were formed inside the islands. When the humidity is increased again to 35%, a recovery takes place by advance of the edges and refilling of the holes. However, despite this partial reversal in the evolutionary trend, the islands tend to disappear in the long run, even when the humidity is kept fixed.

Another interesting observation is that, when the RH is decreased to <20%, the islands evaporate quickly and completely so that no contrast can be observed in the SPFM images. If, however, the humidity is increased again, we sometimes found new islands forming in the same areas that were previously occupied by islands at high humidity. This suggests that some residual condensate might have been formed upon drying, perhaps K_2CO_2 crystals formed by reaction of CO_2 in the atmosphere with the K^+−water surface film, as suggested by some authors.[25,26] Crystallites of these materials could be the nuclei for the subsequent condensation of water. Despite repeated attempts, however, we could not detect such residual material in contact or noncontact images.

High-Humidity (RH > 45%) Regime. At a relative humidity >45%, a brief contact time produces effects similar to those described in the previous section. An interesting difference with the lower humidity regimes is that the structures formed in the modified area appear to be mobile, as shown in Figure 10. The two islands in Figure 10a were produced by two consecutive contacts. Their edges are no longer polygonal and evolve to a more rounded shape. In addition, the islands move relative to each other as shown in Figure 10b−d. Because

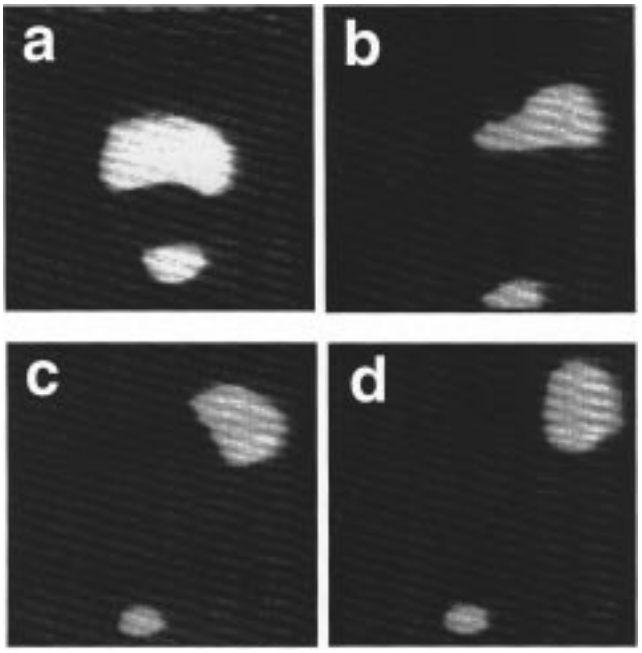

Figure 10. Islands of water formed after two brief tip contacts (<1 s) at high humidity (58%, in this case). The 3 μm × 3 μm SPFM images shown here illustrate the more rounded shape of the islands and their mobility as a function of time. From top left to bottom right, the elapsed time is ~1 h. A slow decrease in size is observed as well.

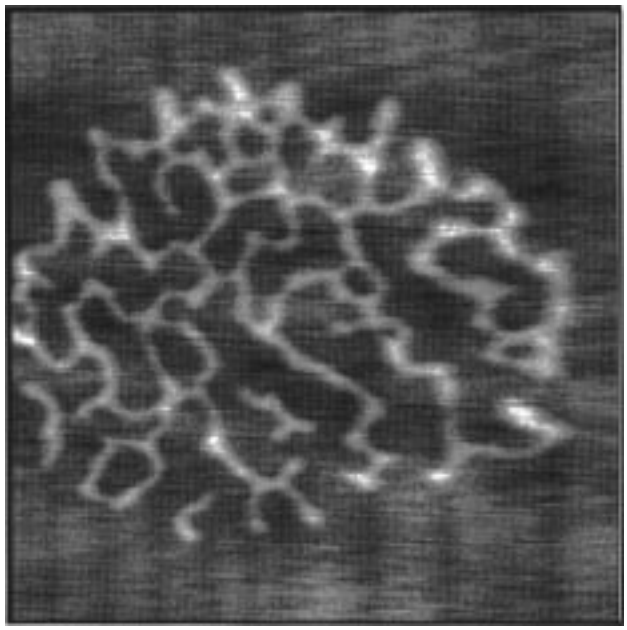

Figure 11. Network of interconnected water channels formed after 5 s of contact of the tip at 40% RH, with a partially contaminated mica surface. The contamination is the result of exposure to the ambient air for ~2 h. Notice that many angles between the segments are close to 120°. The extent of these channel structures increases with contact time.

of the higher humidity level, they also stay on the surface for longer time periods.

Effects of Contamination. Most of the experiments described above were performed on freshly cleaved samples. If the surface had been exposed to air for several hours, the modified area does not show the flat and contiguous islands shown in Figures 6, 8, and 9. Instead, structures resembling a network of interconnected narrow strips or channels, such as the one shown in Figure 11, are formed. Their spatial extent is also dependent on the contact time. These structures disappear with time in a similar fashion as in the previous cases. The geometry of the channels is quite interesting, as they seem to form interconnected segments at angles of 120°. This is another manifestation of the angular epitaxy between the water structures and the mica lattice. At high humidity (≥50%), capillary droplets forming finite contact angles can be seen on the surface for a few minutes before evaporating, as shown in Figure 3.

Discussion

We begin the discussion by discarding any wear-type modification of the mica as the mechanism for the formation of the structures observed after tip contact. This was verified by large area contact AFM images acquired at low load (<10 nN) which showed no change in the topography of the mica. We also know from previous studies of the frictional properties of mica that the threshold force that produces damage is in the range of hundreds of nanonewtons,[27] well above the forces applied in the contact experiments reported here (<1 nN). The mechanical damage produced by large loads is in the form of 10 Å deep holes corresponding to the removal of one mica monolayer. The growth of the modified region with contact time, until it covers an area several orders of magnitude larger than that corresponding to the physical contact between tip and surface, is also clear proof that no mechanical modification took place.

As will be discussed in more detail below, the effect of the contact is to modify the water content in the mica surface over a region around the contact point, due to the capillary action of the tip. At high humidity (>20%), water is added to the surface, while at low humidity there might be loss of water by transfer to a hydrophilic tip. Before discussing the results of the structure and properties of the modified water film, we will comment about the effect of water, whether adsorbed directly from the gas phase or artificially added by contact, on the mobility of the surface ions.

Frequency Dependence and Ion Mobility. The large contribution to the polarization force of slow processes, with a frequency response ranging from 0.1 Hz to several kilohertz (see Figure 5), indicates that in this range the contrast in SPFM is largely due to the diffusion of surface ionic species, as already discussed in our previous work. In muscovite mica, surface ions mainly include K^+, which are exposed upon cleavage and have been detected with many techniques.[28] Other ions, including H^+ from adsorbed water and probably other ions from contamination or arising naturally as minor components of the mica, might be present as well. The formation of hydration shells around these ions should strongly decrease their electrostatic interaction with the substrate, thus lowering activation barriers for surface diffusion. The rapid change in the SPFM frequency response with humidity could then be explained by increasing solvation and consequent increasing mobility of the surface ions as the humidity increases. Frequency response curves, such as those of Figure 4, can in principle be used to determine mobility and concentration of ions on the surface, a subject of great significance in studies of wetting and corrosion that we are actively pursuing. Our results in this subject will be presented in a future publication.

In the present context, reference should be made to the work of Guckenberger et al.[29,30] These authors found that, in humid environments, mica can sustain a current of electrons of >500 pA at 80% RH, flowing from the metallic tip of their STM to the mica sample. They found that this current decreases nearly exponentially with decreasing humidity, down to 0.1 pA at 20% RH. Transport of protons through a H-bonded network of water

molecules was proposed as the conductivity mechanism. Since conductivity s and mobility m are related through $s = nm$, n being the charge concentration, it is interesting to compare their data with the cutoff point in the curves of Figure 4. The comparison shows that conductivity and force frequency response are strongly related, since they change less than a factor of 10 over a change of 5 orders of magnitude in conductivity, as the humidity changes from 10 to 80%.

Thickness of Water Layer vs Humidity. The results of the measurement of the pull-off force in Figure 1 are a good starting point to discuss the effect of humidity on the thickness of the water layer. The fact that the pull-off force remains relatively small below 20% RH indicates that capillary forces do not play an important role at these low-humidity values and that the force is mostly due to adhesive short-range forces. Capillary forces, however, become very important above 20% RH. Above this value, phase II islands were formed after a tip contact, while below 20% only "dielectric holes" were formed (Figure 5). In view of this, we propose that 20% RH corresponds to the saturation of a strongly bound water layer. It is possible that this strongly bound water layer is ordered as in an ice bilayer, as predicted in a recent molecular dynamic simulation.[31] According to that simulation, the K^+ ions remain attached to the mica lattice and are simply covered by a network of H-bonded water.

Contact with the hydrophilic tip above 20% RH gives rise to the condensation of additional water which forms a capillary meniscus around the contact point. Although the thermodynamic equations for capillarity phenomena are derived for macroscopic media where the interfaces can be assumed to be infinitesimally thin, it is still interesting to see how far can they be extrapolated to the molecular size regime. One of the most well-known formulas is the Kelvin equation[23] that relates the Laplace pressure reduction $\Delta p = \gamma/r_1 - \gamma/r_2$ (γ is the surface tension of water and r_1 and r_2 are the concave and convex radius of curvature of the capillary neck, respectively) to the gas-phase change in chemical potential over that of a flat bulk liquid $kT/v \log(p/p_0)$, where k is the Boltzmann constant, T the absolute temperature, v the molecular volume of the liquid, and p/p_0 the relative humidity. At 50% RH, one obtains $r_1 \sim 8$ Å, using 72 mJ/m^2 for γ (if $r_2 \gg r_1$). This negative Laplace pressure, together with that arising from the disjoining pressure of the water film over the mica, determines the thickness of the film in the region around the contact. Far away from it, in the unperturbed mica regions, the thickness is determined by the disjoining pressure alone.[1,2] For mica, the disjoining pressure should be mostly due to the electrochemical double-layer repulsion (dissolution or solvation of K), which can be estimated using well-known formulas.[1,2] For a charge density of ~0.2 C/m^2 the corresponding thickness can be estimated to be ~1 Å at medium humidity (~50%). As indicated above, although they provide useful guidelines for discussion, these formulas and figures should be regarded only as guidelines in the present experiments.[32] They all appear to systematically predict thinner water films than those found experimentally—as seen, for example, in the height of the droplets in Figure 3 (>150 Å), which is substantially larger than the 8 Å radius found above.

The extent and volume of water in the meniscus does not reach equilibrium instantly upon contact but evolves over time, as shown in Figure 2. It increases as the capillary front advances, as seen by the increase in the extent of the areas covered by phase II islands as a function of contact time described above. The time scale of this advance, ~0.1 s at ~40% RH, is comparable to the time response for ionic displacements deduced from Figure 4, indicating that ion diffusion is involved in the formation and expansion of the capillary neck around the contact. This is also in line with the contention that double-layer forces due to ion solvation are at the origin of the disjoining pressure that stabilize the water films. A schematic model illustrating the solvation of surface ions and the expansion of the thicker water films around the capillary meniscus is shown in Figure 13.

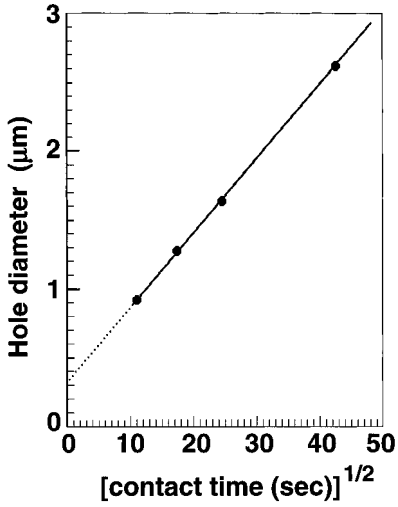

Figure 12. Plot of the diameter of the holes formed by contact at low humidity (14%) as a function of the square root of the contact time. The data correspond to the images in Figure 5. The nearly perfect straight line fit indicates the diffusional origin of the hole formation.

Figure 13. Schematic model illustrating the proposed mechanism of capillary expansion and water film thickness growth under the driving force action of double-layer forces from K^+ ion solvation (dissolution). The finite speed diffusion of the ions outward from the contact point is manifested in the time evolution of the capillary pull-off force and of the lateral expansion of the areas covered by phase II water islands.

Because the residual patches of phase II are long-lived (hours), we propose that the solvation of K^+ is an activated process and occurs most readily when a sufficient amount of water (more than a monolayer) is present. In the presence of excess water, the density of fully solvated K^+ will increase. When the capillary neck is disrupted by retraction of the tip, water evaporates rapidly but still leaves an excess amount of solvated K^+ forming the islands of phase II. This K does not return to its "dryer" state immediately, and equilibrium with the gas-phase pressure is restored very slowly. The details of the molecular scale processes that occur are not clear at present although the images in Figures 8−11 illustrate its effect and spatial distribution.

The decrease of the pull-off force F_{off} as a function of humidity, after it peaks between 20 and 40% RH (Figure 1), can be explained as a simple effect of tip geometry. In macroscopic contacts it is always assumed that r_2, the convex radius of the meniscus is much larger than r_1, the concave one. This assumption leads to the well-known formula $F_{off} = 4\pi\gamma R$ (R = tip radius) for complete wetting situations, which predicts a constant value of the capillary contribution to F_{off}. When nanometer size tips are used, however, the condition $r_2 \gg r_1$ is not necessarily fulfilled, particularly when either of these quantities becomes comparable to the tip dimensions. It is

simple to show that, for a sharp pyramidal tip, for example, r_2 and r_1 become comparable at high humidity, leading to a decrease in Δp, and thus in F_{off}, as observed in our case.

Structure of the Low-Humidity Film. As mentioned above, a strongly bound and ordered water layer is proposed to exist, reaching saturation at $\leq$20% RH. Modification of this film by contact with a hydrophilic tip leaves a rather deep "hole" in the polarizability images (Figure 5). This is not a topographic hole, as demonstrated by the contact AFM images that reveal an unmodified, atomically smooth mica surface. The fact that the contrast of this hole is the same with positive and negative biased tips indicates that the surface potential is the same in the modified and unmodified regions, and therefore it excludes any net transfer of charge between tip and surface during contact. However, ionic exchanges that leave the surface neutral could take place. One possibility is transfer of water (and ions) to the tip in a siphoning process that would decrease even further the contribution of any residual solvated ions that might be present at low humidity.

Whatever their nature, the processes occurring during tip contact appear to be related to diffusion of species on the surface. This can be seen by plotting the diameter d of the holes vs the square root of the contact time. The result is a straight line, as shown in Figure 12, as expected from a simple diffusion mechanism where $r = (4Dt)^{1/2}$. From the slope of this line, the diffusion coefficient for the migrating species is found to be 3.85×10^{-16} m^2/s at 14% RH. From this value, we can also estimate the height of the diffusion barrier. Using the expression $D = \nu a^2 \exp(-E_d/kT)$ for the diffusion constant with $a = 5.2$ Å (mica lattice periodicity) and $n = 10^{13}$ s^{-1}, we obtain $E_d = 0.6$ eV, which is a reasonable value.

Structure of the Water Film >20% RH. The polygonal shape of the boundary of phase II regions, and their orientational registry with the mica lattice, was discussed in detail in a previous work.[18] It suggests an ordered structure for both the first strongly bound layer (phase I) and probably also for the second layer (phase II) water film.

In contrast to the low-humidity case, above 20% RH, the contact potential is substantially increased in the areas occupied by phase II. This could be explained by the increase of the surface dipole moment due to the increased separation of the fully hydrated K^+ ions relative to the negative charges fixed in the mica lattice. Outside the phase II region, most of the K^+ is still directly bound to the mica. In other words, the ions "dissolve" into the water layers to form an electrochemical double-layer structure. It may also be that the concentration of K^+ ions is higher inside phase II as a result of transfer from the surrounding regions. This ion imbalance could be driven by a lower chemical potential of the fully hydrated ions inside the water-rich regions that were created by capillary effects during contact. Besides the contact potential, the ion mobility is also higher inside the phase II islands and accounts for the 2.5 Å polarity independent contrast that remains after the surface potential has leveled off, as shown in Figure 7. Although a more extensive study of the frequency dependence and ion mobility will be presented in a future publication,[33] we can already advance the result that the response due to ionic mobility is faster (by 10−50%) inside phase II islands than outside it (in the phase I regions). This was ascertained by positioning the tip above and outside the islands.

Above 45% RH, we propose that more water is present in the islands so that they become more fluid. This is based on the observation that the islands are no longer polygonal in shape and are more mobile.

Finally, it is interesting to consider the evaporation of the droplets formed after contacts at high humidity in the partially contaminated mica, as in Figure 3. Their shape is very close to a spherical cap, so that their contact angles can be measured from the height and projected diameter. The values found are 2.8°, 2.7°, and 2.3°. Although we have not studied systematically this angle as a function of experimental parameters (temperature, humidity), the observed constant value seems to agree with the predictions by Elbaum et al.[34] for the contact angle of volatile liquids during evaporation. The results illustrate the possibilities of the SPFM imaging mode for capillarity and wetting studies at the nanometer scale, which is the distance scale where surface forces are significant and can therefore lead to a deviation from the macroscopical values. This is particularly true in the case of liquid droplets where no other techniques of comparable resolution are available.

Summary

We have used the hydrophilic tip of an AFM (probably SiO_2 terminated) as a tool to deliver (or to possibly remove) water onto the surface of mica and to modify the structure of the preexisting water film. There are two clear regimes of water coverage at room temperature, one below 20% RH and the other above it. The low-humidity regime is characterized by small pull-off forces exerted on the tip upon retraction and by formation of dielectric holes around the contact point, expanding away from it, depending upon the duration of the contact. This occurs in a time scale of minutes and covers circular areas with diameters of several micrometers. At higher humidity, on the other hand, strong pull-off forces are observed, indicative of capillary condensation around the contact point. The combination of meniscus forces and disjoining pressure from the solvation of K^+ ions forming a double layer produces an affected region that expands away from the contact point over tens of micrometers in a matter of a few seconds. After separation of the tip, two-dimensional islands of water are left on the surface for long times in equilibrium with the vapor. The surface potential is higher inside the islands, an effect that we attribute to the increased dipole from the solvated (dissolved) K^+ ions. Between 20 and 45% RH, the islands are not mobile (except for advances and recession of their edges due to growth or evaporation). They also tend to exhibit straight edges giving them polygonal shapes in registry with the mica lattice directions, suggesting a solid or ice-like structure for the surrounding film (phase I) and perhaps also for the islands (phase II). At humidity levels above 45%, the islands are rounded and mobile, which are suggestive of a more liquid character.

Contamination, accumulating over several hours of exposure to the environment, plays an important role in determining the wettability of mica. It causes the additional water brought by the contact to distribute in a network of more or less straight filaments and producing a finite contact angle ($\sim$2.7°) of water droplets with heights in the tens of nanometers.

We believe that our findings have important implications in the study of interactions between liquids and solid surfaces, wetting, and ionic mobility. The SPFM appears to be an excellent technique to study capillary phenomena in the nanoscale regime.

Acknowledgment. This work was supported by the Lawrence Berkeley National Laboratory through the Director, Office of Energy Research, Basic Energy Science, Materials Science Division of the U.S. Department of Energy, under Contract DE-AC03-76SF00098.

References and Notes

(1) Derjaguin, B. V.; Churaev, N. V. *J. Colloid Interface Sci.* **1974**, *49*, 249.
(2) Pashley, R. M. *J. Colloid Interface Sci.* **1980**, *78*, 246.
(3) Beaglehole, D.; Christenson, H. K. *J. Phys. Chem.* **1992**, *96*, 3395.
(4) Zimmerman, J. R.; Lasater, J. A. *J. Phys. Chem.* **1958**, *62*, 1157.
(5) Christenson, H. K. *J. Phys. Chem.* **1993**, *97*, 12034.
(6) Pashley, R. M.; Israelachvili, J. N. *J. Colloid Interface Sci.* **1984**, *101*, 511.
(7) Porter, J. D.; Zinn, A. S. *J. Phys. Chem.* **1993**, *97*, 1190.
(8) Sposito, G.; Prost, R. *Chem. Rev.* **1982**, *82*, 571.
(9) Ollé, L.; Salmeron, M.; Baró, A. M. *J. Vac. Sci. Technol. A* **1985**, *3*, 1866.
(10) Morgenstein, M.; Michely, T.; Comsa, G. *Phys. Rev. Lett.* **1996**, *77*, 703.
(11) Thiel, P. A.; Madey, T. E. *Surf. Sci. Rep.* **1987**, *7*, 211.
(12) de Gennes, P. G. *Rev. Mod. Phys.* **1985**, *57*, 827.
(13) Leger, L.; Joanny, J. F. *Rep. Prog. Phys.* **1992**, *55*, 431.
(14) Heslot, F.; Cazabat, A. M.; Levinson, P.; Fraysse, N. *Phys. Rev. Lett.* **1990**, *65*, 599.
(15) Cazabat, A. M.; Fraysse, N.; Heslot, F.; Carles, P. *J. Phys. Chem.* **1990**, *94*, 7581.
(16) Hu, J.; Xiao, X.-D.; Salmeron, M. *Appl. Phys. Lett.* **1995**, *67*, 476.
(17) Hu, J.; Xiao, X.-D.; Ogletree, D. F.; Salmeron, M. *Science* **1995**, *268*, 267.
(18) Hu, J.; Xiao, X.-D.; Ogletree, D. F.; Salmeron, M. *Surf. Sci.* **1995**, *344*, 221. Erratum: *Surf. Sci.* **1996**, *355*, 255.
(19) Dai, Q.; Hu, J.; Freedman, A.; Robinson, G. N.; Salmeron, M. *J. Phys. Chem.* **1996**, *100*, 9.
(20) Dai, Q.; Hu, J.; Salmeron, M. *J. Phys. Chem. B* **1997**, *101*, 1994.
(21) Salmeron, M.; Xu, L.; Hu, J.; Dai, Q. *MRS Bull.* **1997**, *22*, 36.
(22) Hertz, H. *J. Reine Angew. Math.* **1881**, *92*, 156.
(23) Carpick, R. W.; Salmeron, M., unpublished results.
(24) See, for example: Adamson, A. W. *Physical Chemistry of Surfaces*; John Wiley & Sons: New York, 1976; Chapter 1.
(25) Bhattacharyya, K. G. *Langmuir* **1989**, *5*, 1155.
(26) Christenson, H. K.; Israelachvili, J. N. *J. Colloid Interface Sci.* **1987**, *117*, 576.
(27) Hu, J.; Xiao, X.-D.; Ogletree, D. F.; Salmeron, M. *Surf. Sci.* **1995**, *327*, 358.
(28) Braun, W. L. *Surf. Interface Anal.* **1980**, *2*, 145.
(29) Guckenberger, R.; Heim, M.; Cevc, G.; Knapp, H. F.; Wiebraebe, W.; Hillebrand, A. *Science* **1994**, *266*, 1538.
(30) Heim, M.; Cevc, G.; Guckenberger, R.; Knapp, H. F.; Wiebraebe, W. *Biophys. J.* **1995**, *69*, 489.
(31) Odelius, M.; Bernasconi, M.; Parrinello, M. *Phys. Rev. Lett.* **1997**, *78*, 2855.
(32) See the discussion in: Israelachvili, J. N. *Intermolecular and Surface Forces*, 2nd ed.; Academic Press: London, 1992; Chapter 12.
(33) Xu, L.; Salmeron, M., to be published.
(34) Elbaum, M.; Lipson, S. G.; Wettlaufer, J. S. *Europhys. Lett.* **1995**, *29*, 457.